International Journal of Thermal Sciences 48 (2009) 1494–1500

Contents lists available at ScienceDirect

International Journal of Thermal Sciences

www.elsevier.com/locate/ijts

Modeling of the in-flight solidification of droplets produced by the uniform-droplet spray process

Suresh Kumar Pillai *, Teiichi Ando

Department of Mechanical and Industrial Engineering, Northeastern University, Boston, MA 02115, USA

ARTICLE INFO

Article history:
Received 6 May 2008
Received in revised form 15 November 2008
Accepted 5 December 2008
Available online 14 January 2009

Keywords:
UDS process
Shielding effect
Recalescence
In-flight solidification

ABSTRACT

A mathematical model to describe the solidification of the droplets produced by the uniform-droplet spray process is developed. The model addresses the motion, heat transfer, nucleation and solidification of traveling droplets. A dimensionless formulation for the interface migration scheme during recalescence is developed. The simulation results of Sn–5wt.%Pb alloy droplets subjected to electrical charging are compared with those in uncharged cases. The effects of charging voltage on scattering and subsequent changes in droplet velocities and heat transfer coefficients are analyzed. The computations show substantial increases in heat transfer coefficient upon charging and notable decreases in droplet velocities and cooling rates.

1. Introduction

The uniform-droplet spray process, also known as the UDS process [1], involves atomization of a laminar jet of molten metal into mono-size droplets by the application of controlled vibration on the jet. A schematic of the process is shown in Fig. 1. In this process, the material to be processed is melted in a crucible under inert atmosphere and the melt is ejected through an orifice as a laminar jet. Perturbations of known frequency are imposed on the jet via a piezoelectric transducer to facilitate controlled capillary break-up of the jet into mono-size droplets. The droplets are electrically charged to prevent their in-flight merging [1,2]. Unlike droplets produced by conventional inert gas atomization, which have different sizes and characteristics, mono-size droplets produced by the UDS process have virtually identical thermal histories and physical and microstructural characteristics [1–3]. Thus, rapid solidification effects can be harnessed with precise microstructural control, thereby making this process an interesting candidate for the production of novel particulates and bulk deposits. Mono-size balls of diameters varying from 50 to 2000 μm have been produced by the UDS process. Their commercial use has so far been realized mainly in electronics packaging applications [3].

Previous models of the solidification of moving droplets [5,6] were mainly concerned with those of gas atomization. These models consider the thermal histories of individual droplets in the atomizing gas. In the UDS process droplets, monosize individual droplets, generated by capillary jet breakup, are coaxially aligned initially and will thus experience a reduced drag force due to shielding effects, which will in turn result in lower heat transfer coefficients. Therefore, the traditional models of gas atomization cannot be applied.

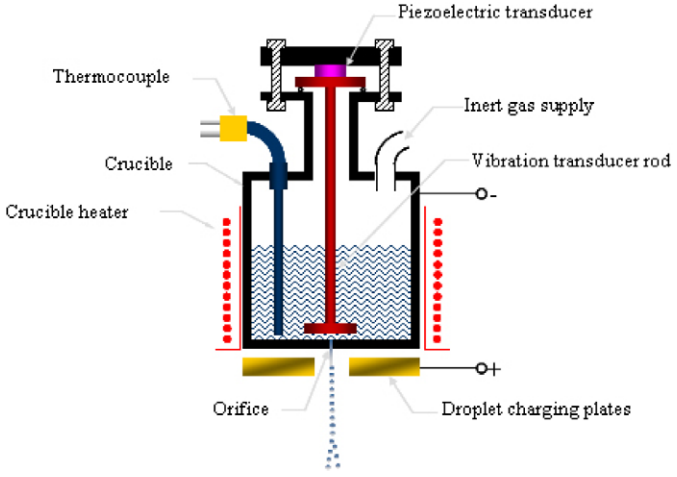

Fig. 1. Schematic of the UDS process.

An in-flight solidification model for the UDS process was first described by Passow [1] and was modified in later works to address the solidification of undercooled alloy droplets [4]. While Passow treated the droplet solidification with zero undercooling followed by isothermal post-recalescence, later works addressed droplet recalescence while using undercooling as an input parameter. The present model uses an in-situ calculation of nucleation

* Corresponding author. Tel.: +1 617 373 2253; fax: +1 617 373 2921.
E-mail address: suresh@coe.neu.edu (S.K. Pillai).

1290-0729/$ – see front matter
doi:10.1016/j.ijthermalsci.2008.12.011

Nomenclature

g	acceleration due to gravity	$m\,s^{-2}$
a	empirical drag coefficient parameter	
C'	capacitance per unit length	$F\,m^{-1}$
C_d	drag coefficient of droplet	
C_{d_A}	drag coefficient of aligned stream of droplets	
C_{d_r}	weighted average of drag coefficients, C_{d_A} and C_{d_s}	
$C_{d_{rod}}$	drag coefficient of a very long rod	
C_{d_s}	drag coefficient for single, spherical droplet	
C_{d_1}	drag coefficient for $\lambda_d/d_d = 1$	
$C_{d_{1+}}$	drag coefficient for droplet spacing relative to λ_d/d_d	
$c_{p(d)}$	specific heat of droplet	$J\,kg^{-1}\,K^{-1}$
$c_{p(g)}$	specific heat of UDS chamber gas	$J\,kg^{-1}\,K^{-1}$
$c_{p(g,f)}$	specific heat of gas evaluated at film temperatures	$J\,kg^{-1}\,K^{-1}$
C_p^x	specific heat of pure "x"	J/kg K
d_d	droplet diameter	m
d_i	distance solid–liquid interface has migrated since nucleation	m
f_s	solid fraction of droplet	
h_{dg}	droplet-to-gas convective heat transfer coefficient	$W\,m^{-2}\,K^{-1}$
$h_{dg,\text{aligned}}$	droplet-to-gas convective heat transfer coefficient for quasi-aligned stream	$W\,m^{-2}\,K^{-1}$
k	partition coefficient	
M	a nucleation parameter	$K^2\,m^{-3}\,s^{-1}$
m_d	mass of single droplet	kg
N	a nucleation parameter	K^3
Pr	gas Prandtl number	
q_d	charge on a droplet	C
Re	droplet Reynolds number	
t	time	s
T	temperature	K
T_d	droplet temperature	K
T_g	chamber gas temperature	K
T_L	liquidus temperature of alloy	K
T_m	melting temperature of pure solvent	K
T_a	ambient temperature	K
V_c	charging cell DC voltage	V
V_i	solid–liquid interface velocity	$m\,s^{-1}$
K_g	thermal conductivity of UDS chamber gas	$W\,m^{-1}\,K^{-1}$
w_c	distance separating charge cell plates	m

Greek symbols

γ	solid–liquid interfacial energy	$N\,m^{-1}$
ΔH_f	latent heat of fusion of alloy	$J\,kg^{-1}\,K^{-1}$
ΔT	total undercooling	K
ε_r	emissivity	
ε	permittivity of the medium	$C^2\,N^{-1}\,m^{-2}$
Φ	time coefficient	s
τ	dimensionless time	
λ_d	droplet break-up wavelength	m
ξ	dimensionless parameter for nucleation position	
μ_g	dynamic viscosity of UDS chamber gas	Pa s
ρ_d	droplet density	$kg\,m^{-3}$
ρ_g	UDS chamber gas density	$kg\,m^{-3}$
σ	Stefan–Boltzmann constant	$W\,m^{-2}\,K^{-4}$
ψ	radius ratio	

Vectors and vector components

$\vec{g}$	gravitational acceleration vector	$m^2\,s^{-1}$
$\vec{r}$	vector representing droplet distance from stream centerline	m
$\vec{r}_{ij}$	distance vector from droplet "i" to droplet "j"	m
$\vec{v}_d$	droplet velocity vector	m/s

Subscripts/Superscripts:

d	subscript, droplet quantity
g	subscript, gas quantity

temperature followed by recalescence using a dimensionless radial dendrite growth scheme, after which segregated solidification takes place according to the Scheil equation [7]. The numerical results obtained under different processing conditions are discussed.

2. Model formulation

2.1. Droplet motion

The droplets are acted upon by the forces of gravitation, aerodynamic drag and buoyancy. The governing equation for the droplet motion can be derived from the force balance to individual droplets as [5,6]:

$$\frac{dv_d}{dt} = g\left(1 - \frac{\rho_g}{\rho_d}\right) - \frac{3}{4d_d} C_d |v_d - v_g|(v_d - v_g) \tag{1}$$

where v_d and v_g are the velocities of the droplet and the gas respectively, g is the acceleration due to gravity; ρ_d and ρ_g are the temperature-dependent densities of the droplet and cooling medium, respectively, C_d is the drag coefficient; and d_d is the droplet diameter. For the UDS-processed droplets subjected to charging and traveling through a static medium, the momentum equation can be modified to:

$$\frac{d\vec{v}_d}{dt} = \vec{g}\left(1 - \frac{\rho_g}{\rho_d}\right) - \frac{3}{4d_d} C_d |\vec{v}_d|\vec{v}_d + \frac{3}{2\pi^2 d^3 \rho_d \varepsilon} \sum_{j=1, j\neq i}^{j=n} \frac{q_d^2 \vec{r}_{ij}}{|\vec{r}_{i,j}|^3} \tag{2}$$

where q_d is the amount of charge per droplet, $\vec{r}_{i,j}$ is the displacement vector between the two droplets i and j in the array, and ε is the permittivity of the medium. For a parallel plate charging arrangement, q_d is determined as the product of capacitance C and the applied voltage. For a parallel plate charging cell, C is given by [8]

$$C' = \frac{2\pi\lambda_d \varepsilon}{0.23 + \ln(\frac{w_c}{d_j})} \tag{3}$$

where λ_d is the break-up wavelength and is the distance between the plates.

To determine the effective drag coefficient, C_d, we employ the scheme used by Passow [1] for a linear array of mono-sized droplets, originally developed by Mulholland et al. [9]. The drag coefficient for a single, spherical droplet, C_{d_s}, is given by [10]:

$$C_{d_s} = 0.28 + \frac{6}{\sqrt{Re}} + \frac{21}{Re} \tag{4}$$

According to Mulholland et al. [9], the drag coefficient, for an aligned stream is given by:

$$C_{d_A} = \left[(C_{d_{1+}})^{-n} + (C_{d_\infty})^{-n}\right]^{-1/n} \tag{5}$$

where n is an empirical parameter ($n = 0.678 \pm 0.07$) and given by $C_{d_{1+}} = C_{d_1} + \frac{a}{Re}(\lambda_d/d_d - 1)$ is the drag coefficient of a sphere relative to the ratio of the droplet break-up wavelength to the droplet diameter. Here, a is another empirical parameter $a = 43.0 \pm 15.4$) and C_{d_1} is the drag coefficient for a droplet when the ratio of droplet wavelength-to-droplet diameter equals one. C_{d_1} is given by [9]

$$C_{d_1} = \left[(C_{d_{\mathrm{rod}}})^{-n} - (C_{d_s})^{-n}\right]^{-1/n} \tag{6}$$

where $C_{d_{\mathrm{rod}}}$ is the drag coefficient for a very long rod, equal to $0.755/Re$. While the radial distance of a droplet from the stream centerline is less than the droplet diameter, a weighted average, C_{d_r}, of coefficients C_{d_A} and C_{d_s} is employed. This is given by [9]:

$$C_{d_r} = \left(1 - \frac{|\vec{r}|}{d_d}\right)C_{d_A} + \left(\frac{|\vec{r}|}{d_d}\right)C_{d_\infty} \tag{7}$$

2.2. Droplet heat transfer

The typical values of Reynolds numbers associated with the UDS process are smaller than that of gas atomized powders owing to stagnant media resulting in smaller Biot numbers compared to the droplets under gas atomization. Hence the temperature distribution inside the droplets may be neglected to assume that the Newtonian conditions prevail. The rate of temperature change within a droplet can then be calculated from [5,6]:

$$\frac{dT_d}{dt} = \frac{\Delta H_f}{c_{p(d)}}\frac{df_s}{dt} - \frac{6h_{d,g}}{\rho_d c_{p(d)} d_d}(T_d - T_a) - \frac{6\sigma\varepsilon_r}{\rho_d c_{p(d)} d_d}\left(T_d^4 - T_a^4\right) \tag{8}$$

where $h_{d,g}$ is the convective heat transfer coefficient between the droplets and the cooling medium, T_d is the droplet temperature, T_a is the ambient temperature, σ is the Stefan–Boltzmann constant, ε_r is the emissivity of the droplet, ΔH_f is the latent heat of the droplet per unit mass, f_s is the droplet solid fraction, and $c_{p(d)}$ is the specific heat of the droplet. The heat transfer coefficient, $h_{d,gi}$ of an isolated droplet can be expressed as [5]:

$$h_{d,gi} = \frac{K_g}{d_d}(2.0 + 0.6Re^{1/2}Pr^{1/3})\left(\frac{c_{p(g,f)}}{c_{p(g)}}\right)^{0.26} \tag{9}$$

where K_g is the thermal conductivity of the chamber gas, $c_{p(g)}$ is the specific heat of the chamber gas, $c_{p(g,f)}$ is the specific heat of the gas at film temperature, and Pr is the gas Prandtl number.

For the cooling in liquid and solid states, appropriate values for specific heats and densities of the liquid and the solid must be used. During solidification, $c_{p(d)}$ and ρ_d are given by the rule of mixing between the properties of liquid and solid.

The laminar momentum and thermal boundary layers can be assumed to behave identically [1], and the heat transfer coefficient is adjusted by the ratio of the effective drag coefficient of the droplet stream to that of an isolated droplet to account for the effects of aerodynamic shielding on the effective heat transfer coefficient [1].

$$h_{d,g} = h_{d,gi}C_{d_r}/C_{d_\infty} \tag{10}$$

By defining a time coefficient, Φ, as $\Phi = -\frac{\rho_d c_{p(d)} d_d}{6h_{dg,r}}$, the critical undercooling, ΔT_c, given by $\Delta T_c = \frac{\Delta H_f}{c_{p(d),l}}$, and by using the heat transfer coefficient representing both convection and radiation, $h_{dg,r}$ given by $h_{d,gr} = h_{d,g} + \sigma\varepsilon_r(T_d + T_a)(T_d^2 + T_a^2)$, Eq. (8) may be rewritten as:

$$\frac{dT_d}{dt} = -\frac{T_d - T_a}{\Phi\left(1 - \Delta T_c \frac{df_s}{dT_d}\right)} \tag{11}$$

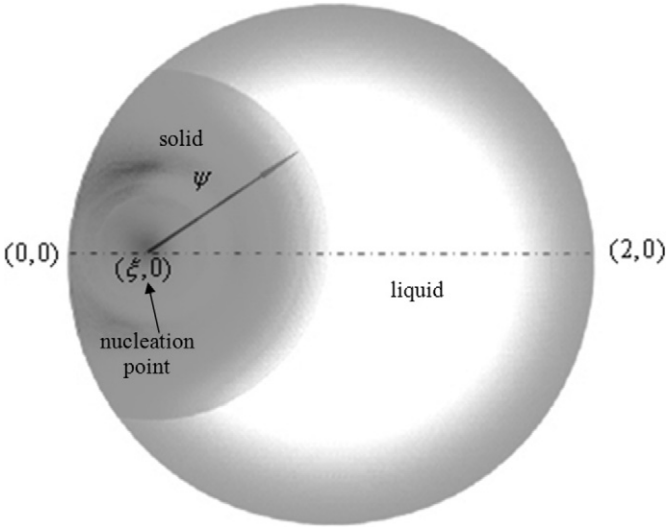

Fig. 2. Interface migration scheme.

2.3. Nucleation

The nucleation temperature has been formulated based on classical nucleation theory, using experimentally determined material constants M and N defined in [11]

$$V_d \int_{T_L}^{T_n} \frac{M}{(T_L - T)^2}\exp\left[-\frac{Q}{RT} - \frac{N}{T(T_L - T)^2}\right]\left(\frac{dt}{dT}\right)dT = 1 \tag{12}$$

where M and N are given by

$$M = \frac{8\pi C_S^0(1 - \cos\theta)\gamma^2 T_L^2 D_0}{a_0^4 \Delta H_V^2} \tag{13a}$$

$$N = \frac{16\pi\gamma^3 T_L^2 f(\theta)}{3k\Delta H_V^2} \tag{13b}$$

where $f(\theta)$ is the catalytic potency function, given by $f(\theta) = (2 + \cos\theta)(1 - \cos\theta)^2/4$ with θ being the wetting angle, D_0 is the pre-exponential term of the liquid diffusivity, γ is the solid–liquid interfacial energy, ΔH_V is the latent heat of fusion per unit volume and T_L is the liquidus temperature. The values of M and N can be determined from controlled droplet nucleation experiments [11].

2.4. Recalescence

The recalescence of the droplets can be modeled based on energy balance arising from the radial growth of a nucleus a point on the surface [12]. A more generalized approach with this assumption was given by DiVenuti where an arbitrary nucleation point inside the spherical droplet was considered [4]. The present work uses a dimensionless formulation of this scheme, illustrated in Fig. 2, where the nucleation point within the droplet $(\xi, 0), 0 \leqslant \xi \leqslant 1$, in the droplet of unit radius centered at $(1, 0)$. By using transformations on dendrite tip velocity, V_i and time, t as $v_i = V_i/r_d$ and $\tau = t/\Phi$, respectively, the 'solidified volume'[1] is a sphere for $\psi \leqslant \xi$, the surface area and the solid fraction of which are given simply by

[1] It should be noted that Eq. (14b) does not account for the interdendritic liquid in the solidified volume. Correction can be readily achieved by dividing f_s by the fraction solid of the solidified volume [13].

$$A_i^S = 4\pi\psi^2 \tag{14a}$$

$$f_s = \frac{4}{3}\pi\psi^3 \tag{14b}$$

The rate of fractional growth of solid may be obtained as

$$\frac{df_s}{dt} = \frac{A_i^S v}{V_d} \tag{15}$$

yielding,

$$\frac{df_s}{d\tau} = 3\Phi v_i \psi^2 \tag{16}$$

For $\psi > \xi$ however, the interface will take a geometric shape depicted in Fig. 2. In this case, the expressions for the interface area and fraction solidified are the same as those of an asymmetric convex lens and are given by

$$A_i^S = 2\pi\psi\left[\frac{1-(\psi+\xi-1)^2}{2(1-\xi)}\right] \tag{17}$$

$$f_s = \frac{(\psi+\xi)^2(\xi^2-2\psi\xi-3\psi^2-4\xi+8\psi)}{16(1-\xi)} \tag{18}$$

also,

$$\frac{df_s}{d\tau} = \frac{3\Phi v_i\psi}{2}\left[\frac{1-(\psi+\xi-1)^2}{1-\xi}\right] \tag{19}$$

In view of Eqs. (11), (20) and (23), the governing equations for recalescence can be expressed as,

$$\frac{dT_d}{dt} = \Delta T_c \frac{6V_i\psi^2}{d_d} - \frac{T_d - T_a}{\Phi}, \qquad \psi \leqslant \xi, \tag{20a}$$

$$\frac{dT_d}{dt} = \Delta T_c \frac{3V_i\psi}{d_d}\left[\frac{1-(\psi+\xi-1)^2}{1-\xi}\right] - \frac{T_d - T_a}{\Phi}, \quad \psi > \xi \tag{20b}$$

The recalescence temperature, T_r and the corresponding fraction solidified, $f_{s,r}$ can be determined from the condition that the internal and external heat fluxes are equal, i.e., $\frac{dT_d}{dt} = 0$.

2.5. Post-recalescence solidification

Further solidification is modeled with the Scheil equation [7] by assuming no diffusion in solid and complete diffusion in liquid. This gives [12],

$$\frac{df_s}{dT_d} = \frac{-(1-f_{s,r})}{(1-k)(T_s - T_{d,r})}\left(\frac{T_s - T_d}{T_s - T_{d,r}}\right)^{(k+2)/(k-1)} \tag{21}$$

where k is the partition coefficient and T_s is the solidus temperature. In view of Eq. (11), the post recalescence solidification is governed by

$$\frac{dT_d}{dt} = -\frac{T_d - T_a}{\Phi\left[1 + \Delta T_c \frac{1-f_{s,r}}{(1-k)(T_s-T_{d,r})}\left(\frac{T_s-T_d}{T_s-T_{d,r}}\right)^{(k+2)/(k-1)}\right]} \tag{22}$$

where T_s is the melting temperature of the pure solvent. Upon reaching the eutectic temperature, T_e, the droplet undergoes isothermal eutectic solidification. The solid fraction is determined by

$$\frac{df_s}{dt} = \frac{T_e - T_a}{\Phi\,\Delta T_c} \tag{23}$$

3. Results and discussion

The model has been applied to a Sn–5Pb alloy. Droplets of sizes varying from 100–500 μm with an initial superheat of 100 K under no charging and applied voltages of 250 and 1000 V are considered in this numerical study. The aforementioned equations for thermal history were solved using a 4th order Runge–Kutta scheme. The thermophysical parameters of argon, the inert gas considered for these computations, and the alloy are given in Tables 1 and 2. The nucleation data for internal nucleation, needed to calculate the values of M and N in Eq. (12), were obtained from the UDS data of this alloy from the works of Wu and Ando [11]. The integration in Eq. (12) is performed along the cooling path of the droplets calculated with Eq. (8) and the nucleation is set to occur when the nucleation probability reaches unity, i.e., Eq. (12). To model the recalescence behavior, a regression data for the dendrite growth velocities of the alloy was obtained from DiVenuti [4]. An asymmetric nucleation position with ξ as 0.25 is chosen for these calculations. The value of partition coefficient, k, required in Eq. (27) was determined from the Sn–Pb phase diagram.

Table 1
Thermophysical parameters of Sn–5Pb [14].

ρ_d	($kg\,m^{-3}$)	7448
$c_{p(d)}$	($J\,kg^{-1}\,K^{-1}$)	736
T_L	(K)	497.7
ΔH	($J\,kg^{-3}$)	57008

Table 2
Thermophysical parameters of argon [15,16].

ρ_g	($kg\,m^{-3}$)	$335.55T^{-0.9971}$
$c_{p,g}$	($J\,kg^{-1}\,K^{-1}$)	$0.182T + 978.0$
μ	($kg\,m^{-1}\,s^{-1}$)	$7.79\times10^{-5}T^{0.6766}$
k	($W\,m^{-2}\,K^{-1}$)	$3.44\times10^{-4}T^{0.7909}$

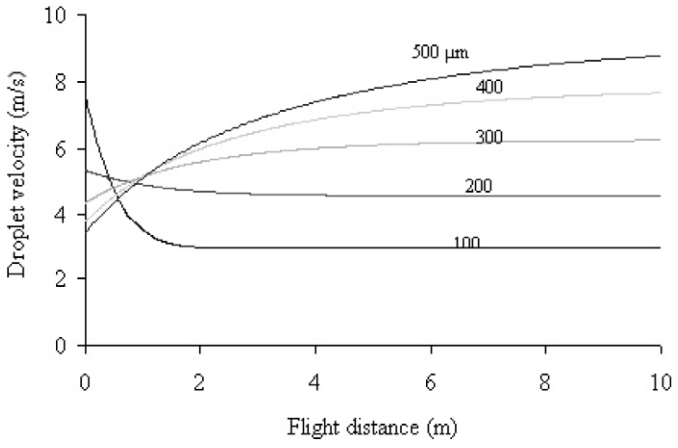

Fig. 3. Velocity of uncharged droplets as a function of flight distance.

Fig. 3 shows the variations in velocity with respect to the distance traveled by 100–500 μm droplets. Owing to the largest value of surface area to mass among the aforementioned droplet sizes, the 100 μm droplets are decelerated to the greatest extent due to drag and attain a terminal velocity at the earliest. According to the simulations, the 200 μm droplets also undergo reduction in velocity during flight. The effect of drag force is less pronounced in larger droplets, 300–500 μm in diameter, which are initially accelerated before attaining a constant velocity.

The heat transfer coefficients of 100 and 200 μm droplets decreases monotonically during flight. The convection heat transfer coefficients of the droplets, Fig. 4, show a strong dependence on the Reynolds number. This suggests that other factors, such as the variation of the shielding effect resulting from the motion of droplet array and the influence of gas viscosity, have negligible influence on the convection during flight.

Fig. 5, showing the temperature as a function of flight distance, is a direct result of the evolution of the droplet velocity and the convection coefficient. The undercoolings achieved by the droplets

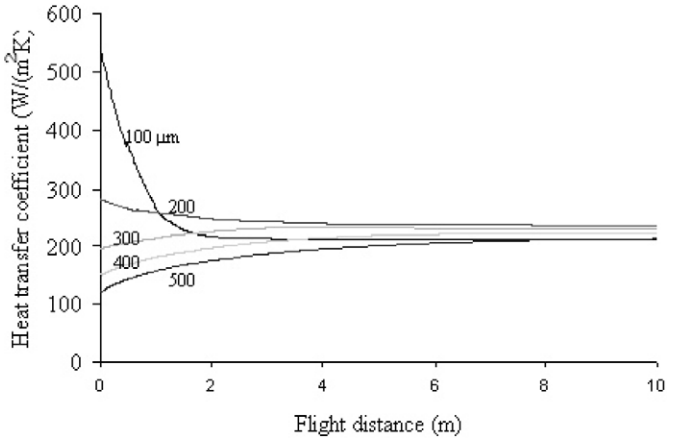

Fig. 4. Heat transfer coefficient of uncharged droplets as a function of flight distance.

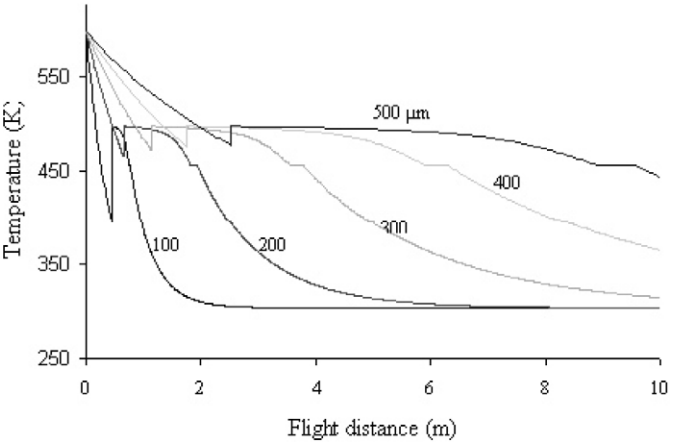

Fig. 5. Thermal history of uncharged droplets.

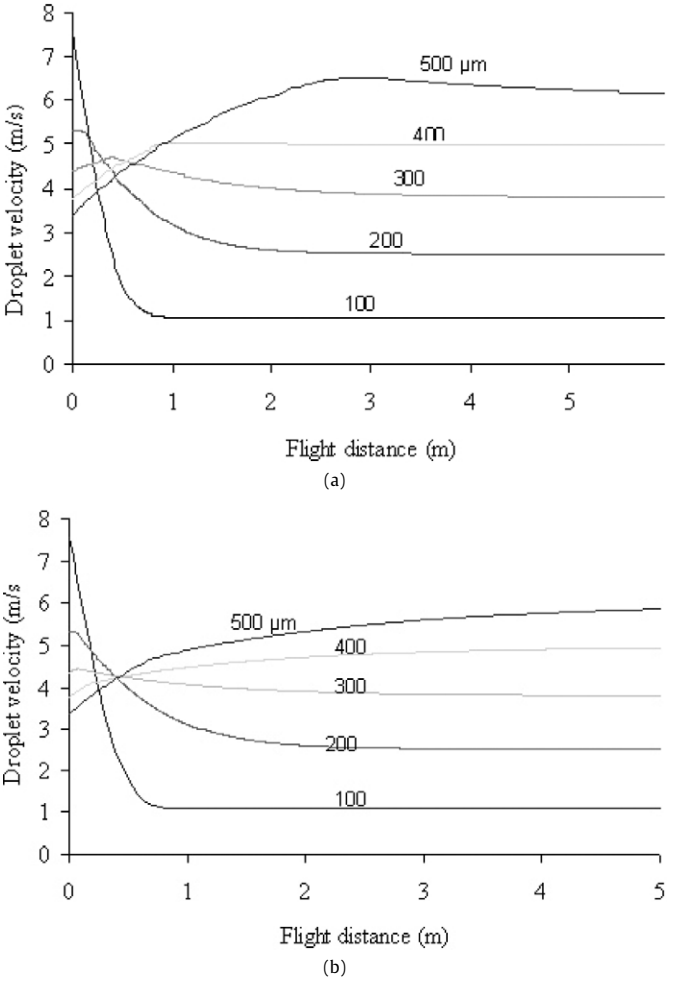

Fig. 6. Droplet velocity as a function of flight distance for droplets charged at (a) 250 V, (b) 1000 V (plate width = 3 mm).

depend strongly on their cooling path and were calculated to lie between 101 K for 100 µm droplets and 21 K for 500 µm droplets. This is followed by the droplet recalescence which is characterized by an abrupt increase in its temperature. The rate of heat removal during the post-recalescence solidification, according to Eq. (22), is smaller than that prior to nucleation due to latent heat release in the post-recalescence stage.

In the present study, computations were done for charging voltages of 250 and 1000 V applied across a parallel capacitor of width 3 mm. The corresponding field strengths are 1.67×10^5 and 6.67×10^5 $V\,m^{-1}$ respectively. The effects of charging on the droplet motion and cooling are found to be significant. Fig. 6(a) shows the velocities of droplets negatively charged at 250 V while Fig. 6(b) shows droplet velocities calculated for charging at 1000 V. The velocity of coaxial droplets, which occur at small flight distances, is greater than that of isolated droplets due to the collective drag reduction. The resulting increase in drag force is responsible for the lower droplet velocities obtained in Figs. 6(a) and 6(b) compared to the uncharged condition. Due to the electrostatic repulsion of charged droplets, the drag force can increase substantially as the motion of the droplets tends to reach that of isolated spheres with larger drag coefficients. Figs. 6(a) and 6(b) show 300 µm droplets undergoing deceleration after initial acceleration due to the aforementioned transition. This transition is relatively faster for droplets charged at 1000 V, Fig. 6(b), than for the droplets subjected to charging at 250 V, Fig. 6(a).

For charged droplets, the shielding effect on the heat transfer coefficient is more severe. Eq. (10) suggests that large amounts of scattering can substantially increase the convection heat transfer coefficient due to the increase in drag coefficients. According to the simulations illustrated in Figs. 7(a) and 7(b), for the droplets charged at 250 and 1000 V, respectively, such increases in heat transfer coefficient can be as much as 150%, due to an increase in the drag coefficient by the same percentage according to Eq. (10). This transition in heat transfer coefficient is achieved more easily by the droplets subjected to 1000 V, Fig. 7(b), owing to the larger amounts of scattering. As in the case with the droplet motion, large amounts of scattering can result in droplets being subjected to convection as isolated particles. The impact of scattering on motion, however, is comparatively lower. This is due to the fact that the effect of drag force on acceleration of the droplets is low at small Reynolds numbers associated with the UDS process.

The simulated thermal histories of the UDS processed droplets under 250 and 1000 V are illustrated in Figs. 8(a) and 8(b), respectively. The droplet cooling rates increase upon charging as a result of increases in convection heat transfer coefficients of the droplets. Larger cooling rates result in increased degrees of undercooling according to Eq. (12). These simulations showed that the droplets of diameter 100 µm undercooled by 104 and 122 K under 250 and 1000 V, respectively. The application of electric charging also resulted in shorter solidification distances; for the largest droplet,

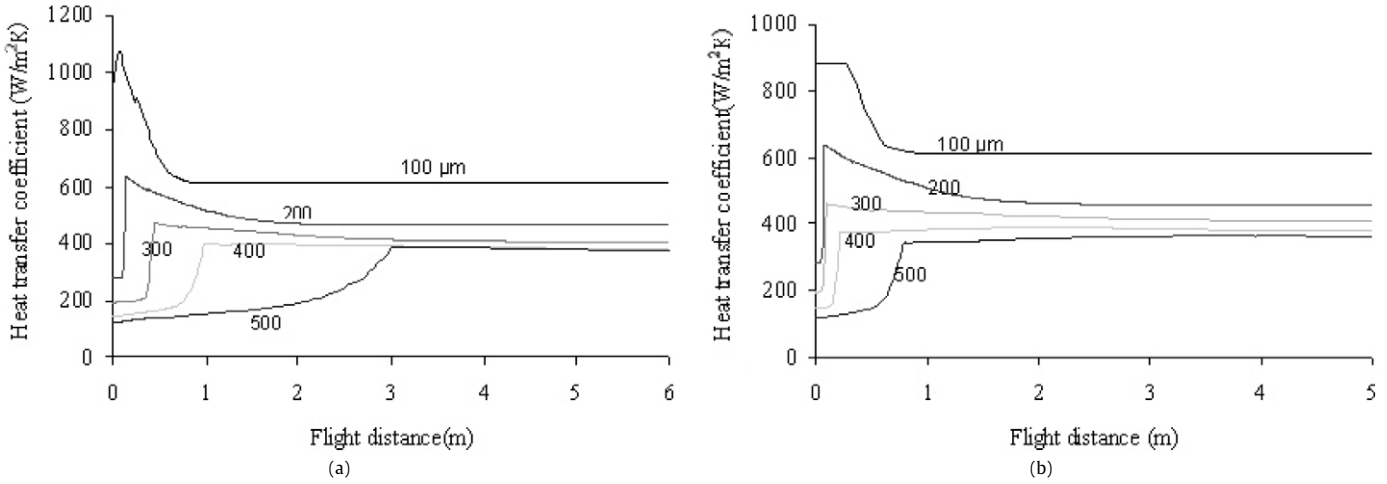

Fig. 7. Heat transfer as a function of flight distance for droplets charged at (a) 250 V, (b) 1000 V (plate width = 3 mm).

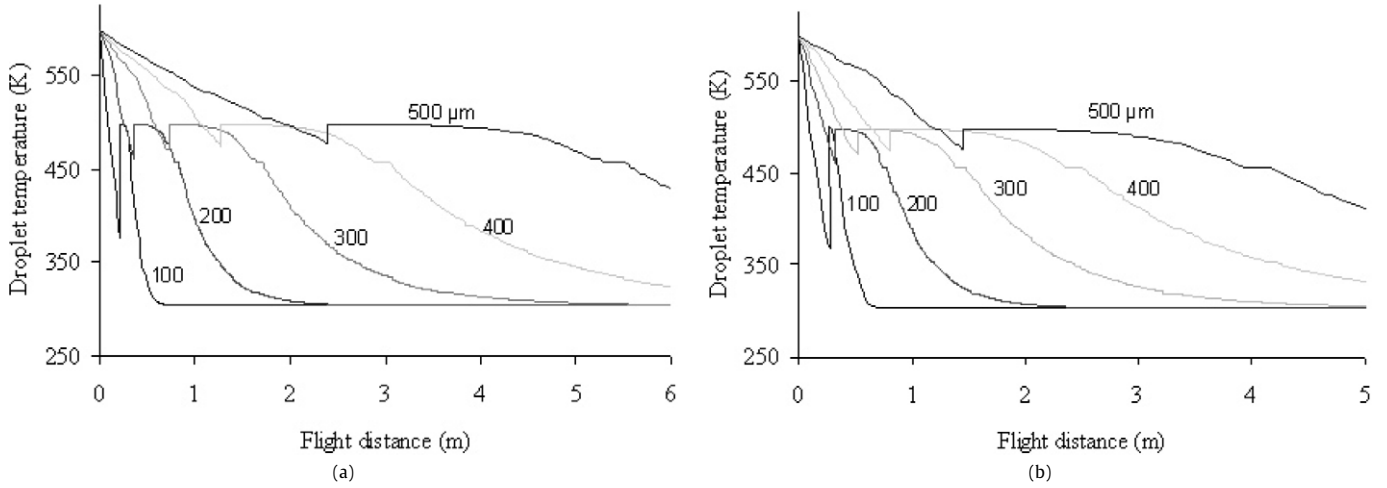

Fig. 8. Thermal history of the droplets charged at (a) 250 V, (b) 1000 V (plate width = 3 mm).

i.e., 500 µm, they were 5.5 and 4.3 m under 250 and 1000 V, respectively.

4. Conclusions

A mathematical model for the heat transfer and motion histories of the UDS-processed droplets was developed under the assumption of Newtonian cooling. It incorporates a droplet nucleation model to calculate the path-dependent nucleation temperature. The recalescence stage is modeled to address the non-equilibrium solidification. The post-recalescence stage is assumed to follow the Scheil conditions, with the final stage occurring isothermally at the eutectic temperature. Dimensionless formulations developed for the droplet recalescence are unique and are applicable to all spherical droplets.

A numerical analysis, performed for Sn–5 wt%Pb droplets, 100–500 µm in diameter produced with and without electrical charging, showed that the motion-controlled parameters of charged droplets undergo a significant transition during droplet flight.

Acknowledgements

This work was supported by Hitachi Metals, Ltd., Japan.

References

[1] C.H. Passow, A study of spray forming using uniform droplet sprays, MS thesis, Massachusetts Institute of Technology, USA, 1992.
[2] J.-H. Chun, C.H. Passow, Production of charged uniformly sized metal droplets, United States Patent #5,266,098.
[3] C.-A. Chen, S. Sahu, J.-H. Chun, T. Ando, Spray forming with uniform droplets, in: Science and Technology of Rapid Solidification and Processing, Proceedings of the NATO Workshop, Kluwer Academic Publishers, Dordrecht, 1995, pp. 123–134.
[4] A. DiVenuti, Characterization of droplet flight path and mass flux in droplet-based manufacturing, MS Thesis, Tufts University, USA, 1996.
[5] P. Mathur, D. Apelian, A. Lawley, Analysis of the spray deposition process, Acta Metall. 37 (1989) 429–433.
[6] P.S. Grant, B. Cantor, L. Katerman, Modelling of droplet dynamics and thermal histories during spray forming. I. Individual droplet behavior, Acta Metall. Mater. 41 (1993) 3097–3108.
[7] E. Scheil, Bemerkungen zur schichtkristallbildung, Z. Metallk. 34 (1942) 70–72.
[8] K.G. Abel, Modeling of in-flight solidification of traveling uniform-droplets, MS Thesis, Massachusetts Institute of Technology, USA, 1993.
[9] J.A. Mulholland, R.K. Srivastava, J.O.L. Wendt, Influence of droplet spacing on drag coefficient in nonevaporating, monodisperse streams, AIAA Journal 26 (1988) 1231–1237.
[10] J. Szekely, Fluid Flow Phenomena in Materials Processing, Academic Press, New York, USA, 1979.
[11] P. Wu, T. Ando, Computation of continuous cooling transformation diagrams for the heterogeneous nucleation in Sn–5 mass pct Pb droplets, Metall. Trans. A 36 (2005) 35–41.
[12] S. Lee, E.-S. Ahn, Solidification progress and heat transfer analysis of gas-atomized alloy droplets during spray forming, Acta Metall. Mater. 42 (9) (1994) 3231–3243.

[13] W.J. Boettinger, L. Bendersky, J.G. Early, An analysis of the microstructure of Al–8 wt% Fe rapidly solidified powders, Metall. Trans. 21A (1986) 781.
[14] C.J. Simithells, E.A. Brandes, Metals Reference Book, Butterworths, London, UK, 1976.
[15] R.C. Weast (Ed.), CRC Handbook of Chemistry and Physics, 68th Edition, CRC Press, Boca Raton, FL, USA, 1987.
[16] J.B. Wiskel, H. Henein, E. Maire, Solidification study of aluminum alloys using impulse atomization: Part 1. Heat transfer analysis of an atomized droplet, Can. Metall. Q. 41 (2002) 97–110.